# EUV Binary Phase Gratings: Fabrication and Application to Diffractive Optics

F. Salmassi,* P.P. Naulleau, E.M. Gullikson, D.L. Olynick and J.A. Liddle

Center for X-Ray Optics, Lawrence Berkeley National Laboratory, 1 Cyclotron Road, Berkeley, CA 94720, USA

keywords: *diffractive optics, EUV, electron-beam, lithography, Nanofabrication*

**Abstract**

Diffractive optics play an important role in a variety of fields such as astronomy, microscopy, and lithography. For the extreme ultraviolet (EUV) region of the spectrum they have been difficult to make due to the extremely precise control required of their surface structure. We have developed a robust fabrication technique that achieves the required topographic control through the deposition of a thin film of Si on a Cr etch stop. We have fabricated binary phase gratings using this approach that have an efficiency of 80% of the theoretical maximum. The technique is applicable to any type of binary phase optical element.

* email: Fsalmassi@lbl.gov

## Introduction

Diffractive optics play an important role in a variety of fields such as astronomy, microscopy, and lithography. For the extreme ultraviolet (EUV) region of the spectrum they have been difficult to make due to the extremely precise control required of their surface structure. This surface structure must be commensurate with the very short wavelength of 13.5 nm. As extreme ultraviolet lithography (EUVL) approaches commercialization the need for high efficiency diffractive optics for this region becomes more and more important.

We recently presented data on both a blazed grating[i] and a diffuser[ii,iii] produced by generating three-dimensional surfaces on a lateral length scale of 100 nm. In both cases, the fabrication process required a lengthy calibration of the resist response and of the response of the multilayer coating to the underlying resist topography before the desired structures could be made. The resist used, hydrogen silsesquioxane (HSQ), having low sensitivity, leads to exposure times in excess of 6 hrs/mm$^2$ for a typical e-beam lithography process. In this paper we discuss a simpler and faster approach to fabricating diffractive optics for the EUV regime and show the results generated using this process to fabricate highly efficient binary phase gratings. The technique is also directly applicable to other diffractive structures for EUVL such as diffusers and shaped illuminators.

## Theoretical Efficiency & Design Requirements

Although less efficient than blazed phase devices, binary phase gratings serve as convenient and relatively efficient carriers for diffractive and holographic optical devices.

Moreover, when dealing with applications where both positive and negative diffracted orders can be used (such as for an optical element intended to produce dipole illumination), theoretical efficiencies upwards of 80% can be achieved. The difficulty in fabricating these devices arises from the requirement to produce topography of precisely 3.4nm to achieve a $\lambda/2$ phase shift upon reflection at EUV. Small variations in phase, duty cycle, and surface roughness have a substantial impact on device performance. To establish a benchmark for grating performance, and to determine the deviations from the ideal that can be tolerated, we must first define efficiency and then look at some theoretical limits for an ideal phase device. Theoretical efficiency is defined here as the $n^{th}$ order diffracted light divided by the total diffracted light. Figure 1 a) shows the theoretical efficiency of an ideal grating with respect to height (phase), and Figure 1 b) shows the theoretical efficiency with respect to duty cycle.

Suppression of the specular reflection component ($0^{th}$ order light) to below 1% means that a height variation no greater than 0.2 nm or a gap period ratio change of only 0.02 from 0.50 can be tolerated. If on the other hand we set our criterion based on less than 10% loss in diffraction efficiency, the height variation must be less than approximately 0.5 nm or a gap period ratio change of 0.1 from 0.50. In addition to this, with the wavelength region of interest being EUV, the overall roughness of the surface after multilayer coating should be no more than 0.3nm RMS to minimize loss due to scattering (ref).

**Grating Fabrication**

In many situations precise dimensional control can readily be achieved by means of thin-film deposition techniques. We therefore chose to use a series of thin films to define accurately and precisely the very small topographic variations needed for our device. In this case, we are free to use a fast, chemically-amplified resist with modest resolution. This leads to a reduction in exposure times by a factor of fifty or more compared with our previous work.

However, in order to satisfy these strict fabrication requirements we also require the right combination of materials and etch chemistry. Silicon was chosen as the material in which to define the topography and chrome was chosen as the etch-stop layer. Cr provides excellent etch selectivity and the Si-Cr system is a good candidate for residue-free pattern transfer,[iv] which is a critical requirement for keeping roughness to a minimum. The films were deposited using DC magnetron sputtering in an argon plasma at a target-to-substrate distance of 3.5 inches. The deposition conditions were optimized for lowstress films, which is important for sharp surface relief profiles.

As mentioned earlier, topography of only 3.4nm is needed to achieve maximum efficiency. However, producing a surface relief of 3.4nm after the completion of all processing steps proves to be not as trivial as merely depositing a thin film. Certain effects, which might typically be considered negligible, make sizable contributions to the final measured height, and, if not corrected for, will quickly consume diffraction efficiency. Interface diffusion or interdiffusion of one film deposited on another film typically causes a contraction in overall film thickness. Surface oxidation of thin films exposed to room air cause an increase in overall thickness. The wet chemistry involved,

namely resist development, and later stripping, in aqueous base (which is known to etch Si[v]), may change the overall thickness by unwanted etching or oxidation of the Si relief film or the Cr etch-stop layer respectively. In addition to these parametersthe exact etch depth through the interdiffusion layer is not well known.

To estimate the Si thickness needed we consider surface oxidation and interdiffusion: 0.46nm of silicon is consumed make a 1.0nm of $SiO_2$ (ref), and we know that for stoichiometric $SiO_2$ that after a week of exposure to room air, $SiO_2$ stops growing at a thickness of 2.5nm (ref). We estimate the interdiffusion of Si into Cr for our purposes at 0.7nm from our experience with a Mo/Si model (ref). Therefore the thickness estimate of silicon required for the surface relief structures is given by

$$\text{Thickness} = \text{sputtered film} + \text{oxide growth} - \text{interdiffusion}$$

Note that this equation does not guarantee the desired step height after the etch, but provides an approximate starting point.

In order to verify this simple model, we developed a facile experimental approach by exposing and processing many gratings of varying thickness on one substrate under similar conditions, thus eliminating multiple iterative experiments. By designing apertures that vary the shape of the sputter plasma incident on the substrate, thin films can be fabricated for a desired uniformity or for a desired non-uniformity. A sputter aperture was designed to vary Si film thickness from 2 nm - 5 nm on a 5 nm Cr etch-stop

layer see Figure 2 a). Recall that two parameters determine grating efficiency, phase and duty cycle. The above approach varies phase, i.e. thickness, along the substrate. The duty cycle was controlled by varying the delivered dose during the lithography step.

An e-beam tool operating at 100kV and 440pA delivering a base dose of 25μC/cm$^2$ was used to expose the diffractive optical elements (DOEs) in IBM's KRS-XE resist. Prior to resist application the substrate containing the Si-on-Cr film was treated with a monolayer of photoresist primer - hexamethyldisilazane (HMDS) - for good photoresist adhesion. A 4.8% formulation of KRS-XE was spun in a conventional commercial spinner at 2000rpm for 60 seconds, resulting in a resist film thickness of approximately 120nm. Four columns of gratings were exposed with doses of 25, 27, 29, and 31μC/cm$^2$ respectively, with each dose column containing 20 binary grating cells of both 200nm and 1000nm period. After exposure the substrate was developed in tetramethylammoniumhydroxide (TMAH Shipley LDD26W) for sixty seconds and rinsed with deionized water.

Etching for pattern transfer was done on an Oxford plasma etcher using a low-energy inductively-coupled $SF_6$ plasma for a residue-free surface relief structure, which is critical for minimizing loss due to scatter. $SF_6$ produces minimal polymer residue, compared to fluourocarbon chemistries, while the low DC bias of the plasma minimizes the chances of producing additional height changes through sputtering of the Cr etch-stop layer. The remaining resist was then removed by a combination of blanket UV exposure and developer soak, followed by an $O_2$ descum. The topography was then investigated

using an atomic force microscope (AFM). Figure 2 b) shows the height measurements of gratings.

Following AFM measurements the gratings were coated with a Mo/Si multilayer designed for near-normal reflection at $\lambda$=13.5nm. Figure 3 a) shows a cross-sectional SEM of the gratings with a multilayer coating designed for conformal growth and Figure 3 b) shows AFM scan of multilayer-coated 1000nm gratings. Although there have been numerous studies[4] to develop deposition techniques which smooth topography (defects) during multilayer deposition, we used a non-smoothing coating in order to conform to the topography precisely and ensure the propagation of the topography along the growth surface so that the phase shift produced was uniform through the multilayer thickness.

**Results & Discussion**

The reflectivity of the multilayer coating was measured to be 65%. Reflectometry was done at the LBNL-CXRO calibration and standards facility at the Advance Light Source (ALS). Figure 4 shows the reflectance of individual 200nm gratings as a function of their height (phase) for the 27$\mu C/cm^2$ dosed column. The results show that the highest measured reflectivity for a grating was 22%. We recall that the maximum theoretical reflectivity for an ideal grating with a 65% multilayer coating is 26% (0.4 x 0.65). Thus the measured efficiency is better than 80% of the theoretical maximum.

The measurements show that the theoretical and the measured curves coincide. Notice the inverse relationship between the $0^{th}$ and the $1^{st}$ orders in the theoretical curves. The $0^{th}$

order (or specular reflection), is expected to increase with diminishing $1^{st}$ order strength. Both the measured $0^{th}$ and $1^{st}$ order plots are skewed to the right and are asymmetrical about the vertical axis. This indicates that for these features the reflected light is lost due to some mechanism. Further measurements of individual gratings also show an asymmetry.

We note that although the measured height of the most efficient grating corresponds to the expected 3.4 nm, the thickness of Si required to produce this was 5.5 nm. This is in contrast to our initial estimate of 3.5 nm. Whether this is due to a larger than expected amount of interdiffusion, or to a loss of Si during the resist removal step is not yet known.

Figure 5 shows a reflectance scan of the highest performing grating. Notice the effective suppression of the $0^{th}$ and $2^{nd}$ orders. The $1^{st}$ orders are above 20%. This indicates good control of duty cycle and phase. However, note the unequal strength of the $1^{st}$ and $-1^{st}$ orders. A cross-section SEM micrograph (Figure 6) of the gratings reveals a possible explanation for this, and the previously described asymmetries. The SEM micrograph shows an off-normal growth of the grating structure through the multilayer volume. The surface topography is not translating normal to the surface but at an angle $\beta$. Gullikson et al.[vi] have documented this phenomenon. During sputter deposition of a multilayer, topography translates along the average direction of incident flux. Since the sputtering plasma is non-uniform, with a radial angular distribution, we see this reflected in the grating topography. Thus for this experiment, features at the edge of the substrate have an inherent phase shift associated with the multilayer coating, which explains the asymmetry. The best performing grating, being off-center, had an incident flux angle $\beta$

≠0. As a result of the phase shifting effect of the multilayer, the 1st and –1st order strengths are not equal.

## Summary

We have shown that binary phase-only optics for EUV can be fabricated with high relative efficiencies. In addition, we have attained some guidelines for device performance and developed a fabrication process by which more sophisticated diffractive and holographic phase devices could be fabricated.


## Acknowledgements

This work was supported in part by DARPA under contract number MDA972-98-C-0007 and by the Director, Office of Science, Office of Basic Energy Sciences, Materials Science and Engineering Division, U.S. Department of Energy under Contract Nos. DE-AC03-76SF00098 and W-31-109-ENG-38.


## References


[i] J.A. Liddle, F. Salmassi, P.P. Naulleau, E.M. Gullikson, "Nanoscale Topography Control for the Fabrication of Advanced Diffractive Optics," *J. Vac. Sci. & Technol. B*, **21**, 2980 (2003). LBNL-53390

[ii] P.P. Naulleau, J.A. Liddle, F. Salmassi, E.H. Anderson and E.M. Gullikson, "Design, Fabrication and Characterization of High-Efficiency Extreme Ultraviolet Diffusers," to appear in *Applied Optics*.

[iii] Patrick P. Naulleau, James A. Liddle, Farhad Salmassi, Erik H. Anderson, and Eric M. Gullikson, Proc. SPIE Int. Soc. Opt. Eng. 5347, 9 (2004)

[iv] Deirdre Olynick, Farhad Salmassi, J. Alex Liddle, "Fabrication and Performance of Nanoscale Ultra-smooth Programmed Defects for EUV Lithography," to appear in J. Vac. Sci. & Technol.

[v] See e.g. M. Madou, "Fundamentals of Microfabrication", CRC Press, Boca Raton (1997)

[vi] E.M.Gullikson, D. G. Sterns, "Asymmetric extreme ultraviolet scattering from sputter-deposited multilayers," Phys Rev. B , 59, 13 273 (1999)

**Figure Captions**

Figure 1. a) Plot of the strength of the $0^{th}$ (specular) and $1^{st}$ order reflections from an ideal binary phase grating as a function of deviation in height. The $0^{th}$ order efficiency varies with grating height, h, as $0.2*\Delta h^2$ where $\Delta h = h-\Delta/4$. b) Plot of $0^{th}$ and $1^{st}$ order strengths from an ideal binary phase grating as a function of gap/period ratio (duty cycle)

Figure 2. a) AFM data taken across a wafer with a graded Si layer showing the control that can be achieved in the Si thickness. b) Cartoon of the wedge geometry

Figure 3. a) Cross-sectional view obtained by SEM of Mo/Si multilayer deposited by DC magnetron sputtering as described here. b) AFM image of 1000 nm period, 3.4 nm height grating after multilayer deposition.

Figure 4. Measurements showing grating performance at 23% absolute, or 80% relative efficiency to theoretical predictions. The $0^{th}$ order measurements are skewed to the right due to off-normal columnar multilayer growth during deposition.

Figure 5. Diffraction data from 200 nm period binary phase gratings showing the absolute diffraction efficiency of the $1^{st}$ and $-1^{st}$ orders. Notice the suppression of the $0^{th}$ order. The peak widths are instrumental in origin. Relative efficiencies are obtained by dividing the absolute efficiency by the multilayer reflectivity of approximately 65%.

Figure 6. During sputter deposition, for non-uniform plasma, the topography translates along the average direction of incident flux.

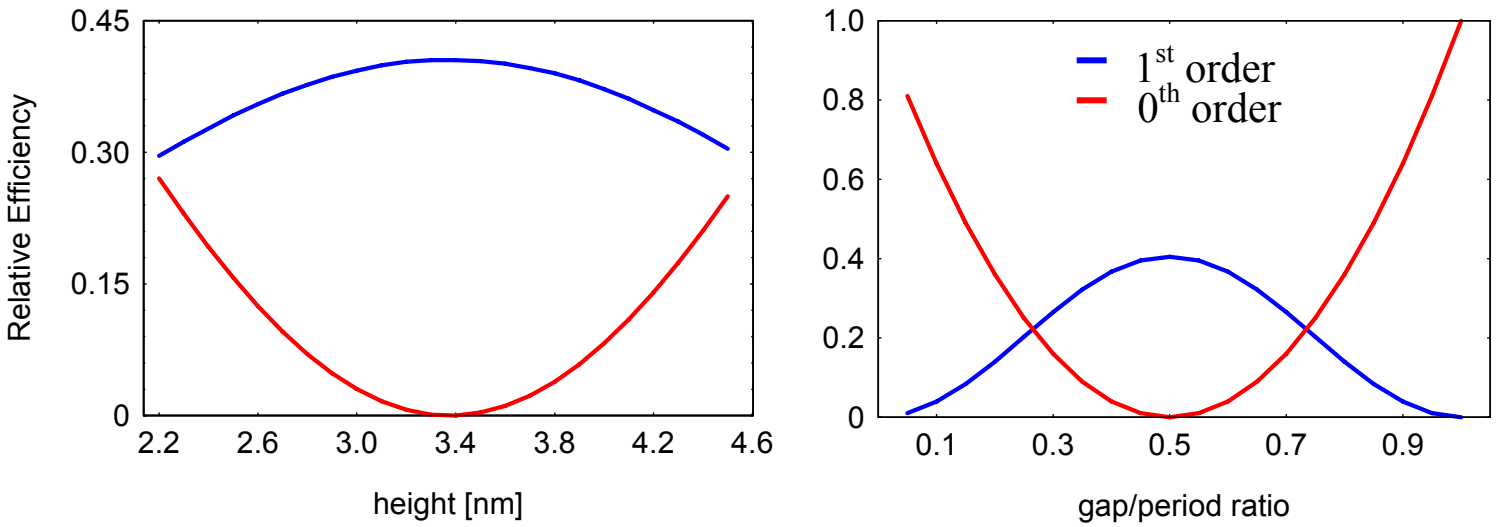


Figure 1. a) Plot of the strength of the $0^{th}$ (specular) and $1^{st}$ order reflections from an ideal binary phase grating as a function of deviation in height. The $0^{th}$ order efficiency varies with grating height, h, as $0.2*\Delta h^2$ where $\Delta h = h-\lambda/4$. b) Plot of $0^{th}$ and $1^{st}$ order strengths from an ideal binary phase grating as a function of gap/period ratio (duty cycle)

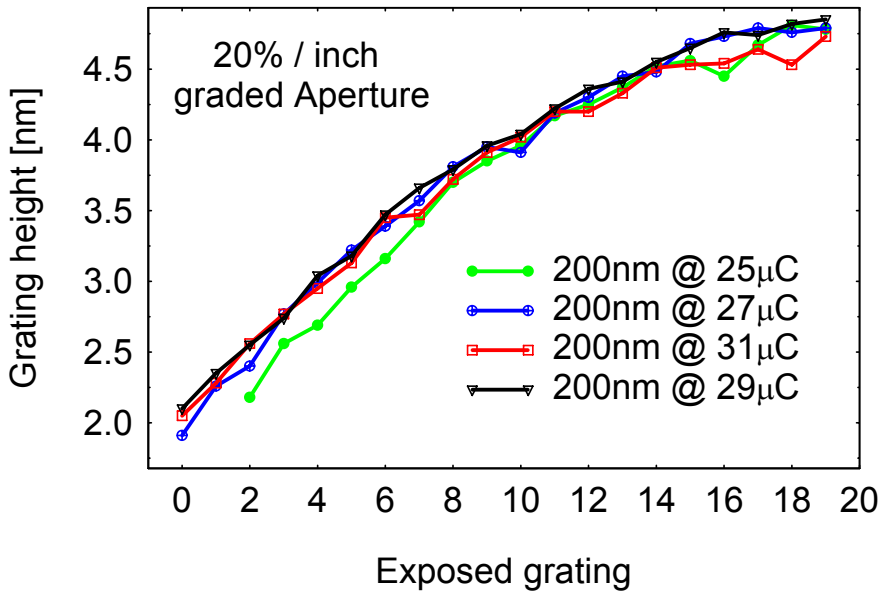


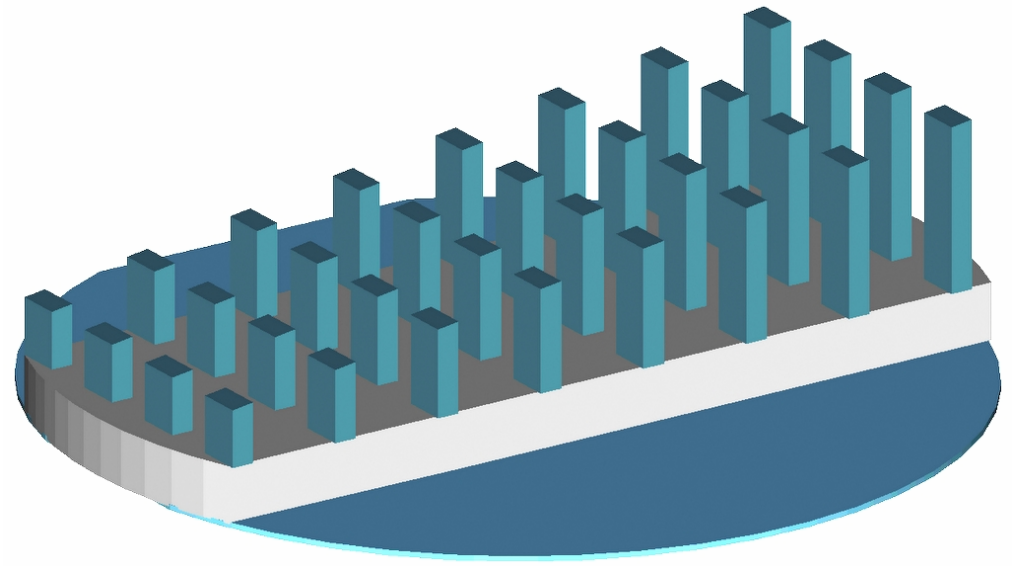

Figure 2. a) AFM data taken across a wafer with a graded Si layer showing the control that can be achieved in the Si thickness. b) Cartoon of the wedge geometry

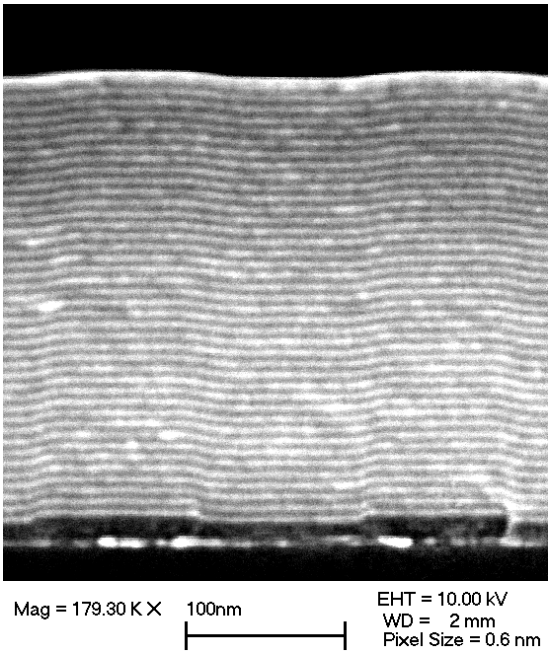


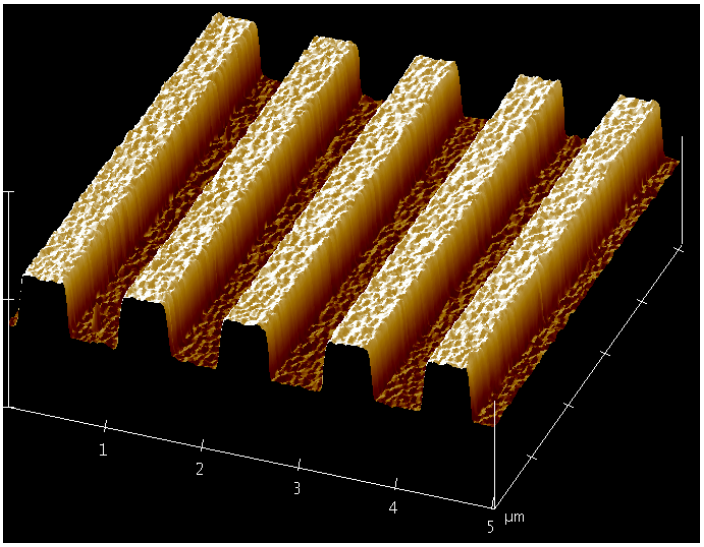


Figure 3. a) Cross-sectional view obtained by SEM of Mo/Si multilayer deposited by DC magnetron sputtering as described here. b) AFM image of 1000 nm period, 3.4 nm height grating after multilayer deposition.

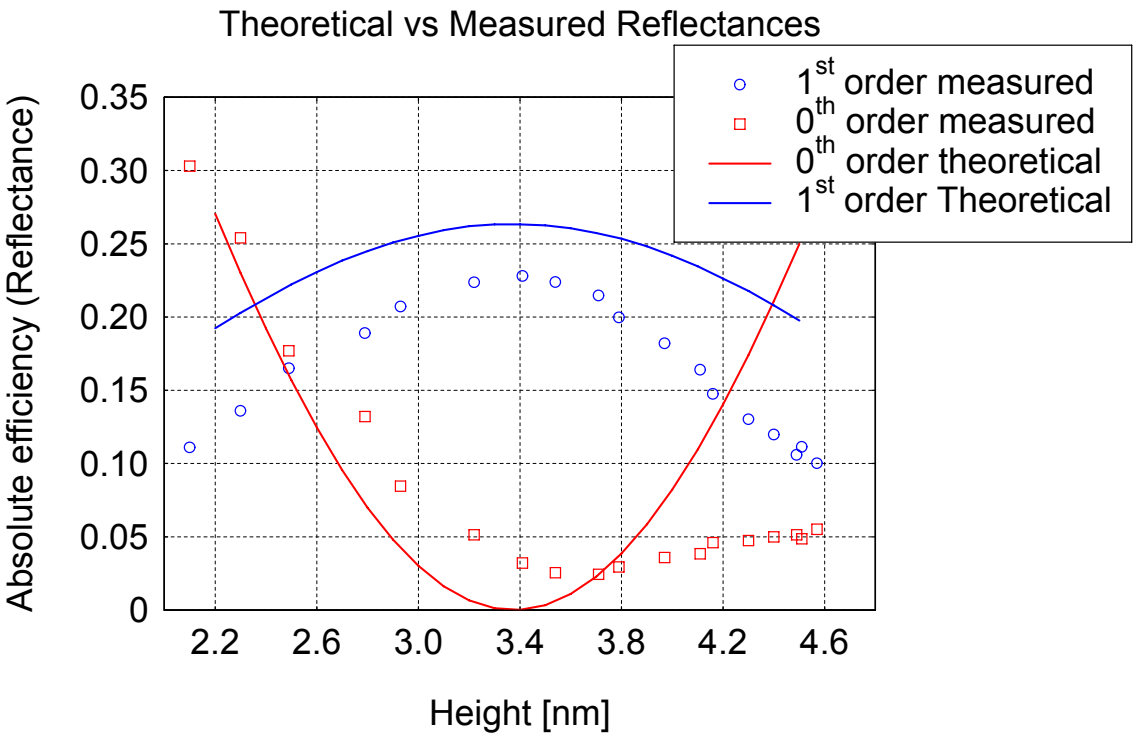


Figure 4. Measurements show grating performance at 23% absolute, or 80% efficiency relative to theoretical predictions. Notice the ~0.3nm measurement offset due to AFM calibration. The $0^{th}$ order measurements skewed to the right due to off-normal columnar multilayer growth during deposition.

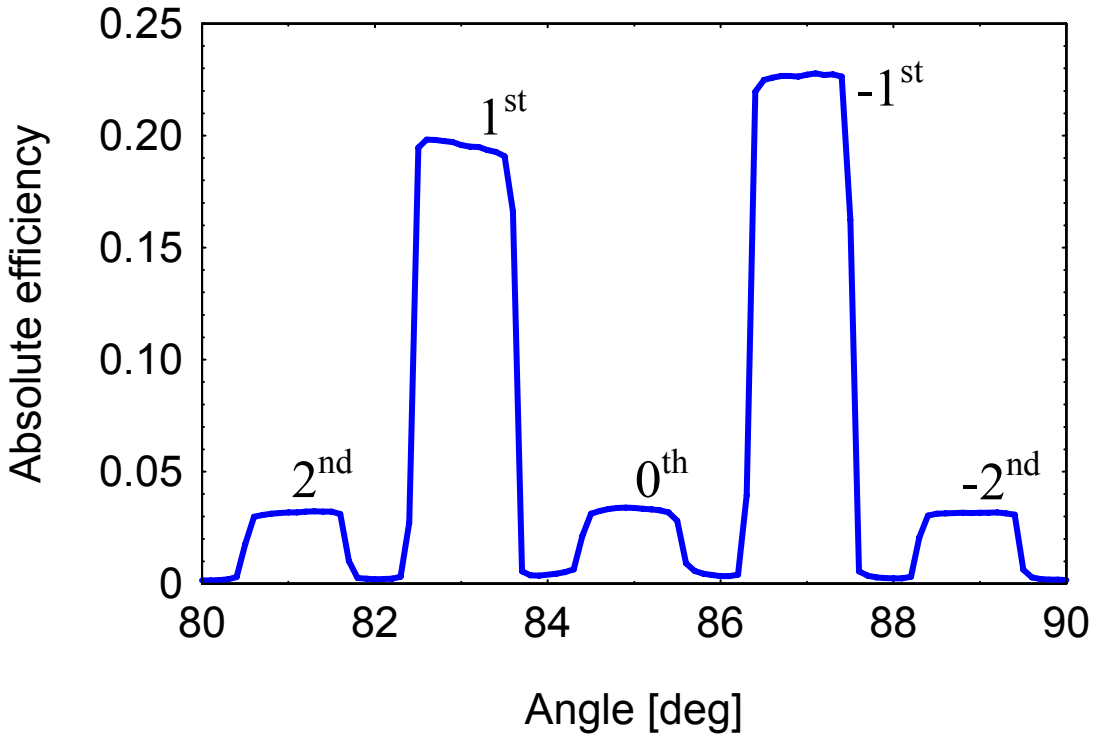


Figure 5. Diffraction data from 200 nm period binary phase gratings showing the absolute diffraction efficiency of the $1^{st}$ and $-1^{st}$ orders. Notice the suppression of the $0^{th}$ order. The peak widths are instrumental in origin. Relative efficiencies are obtained by dividing the absolute efficiency by the multilayer reflectivity of approximately 65%.

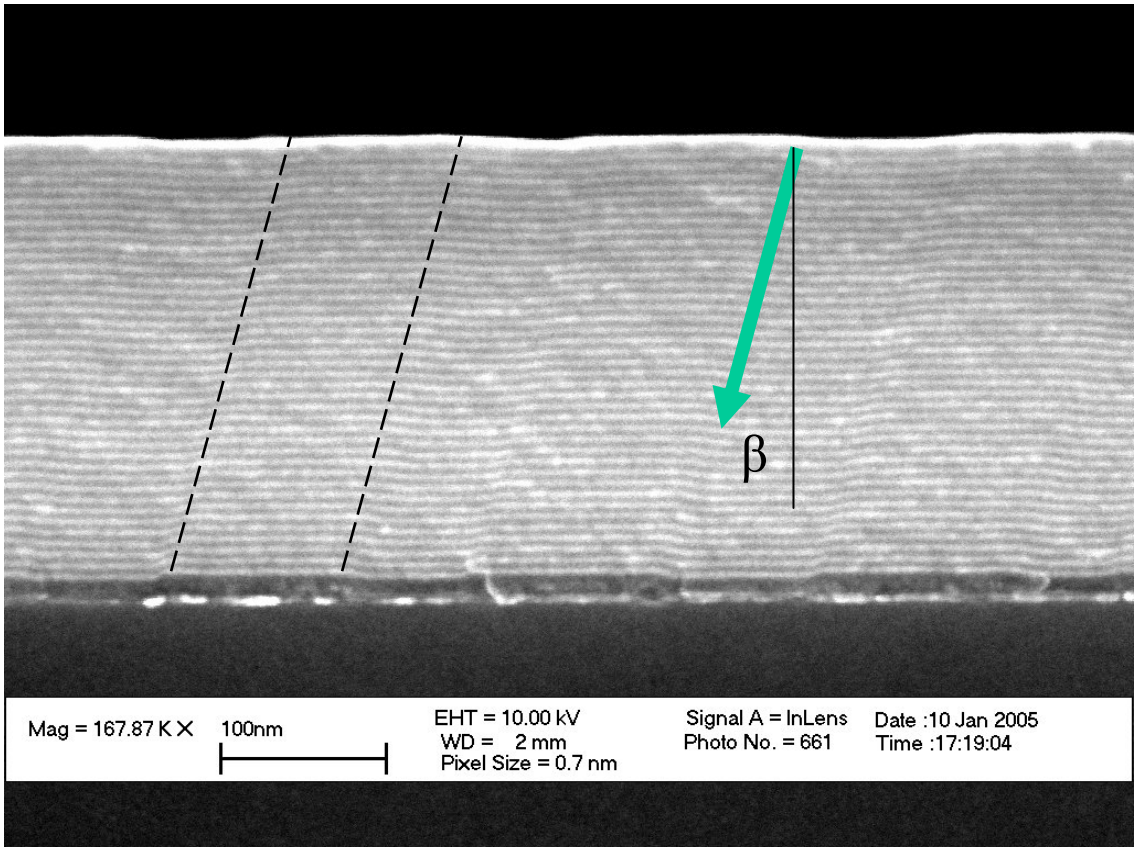


Figure 6. During sputter deposition, for non-uniform plasma, the topography translates along the average direction of incident flux.